Available online at www.sciencedirect.com
ScienceDirect
Hearing Research 228 (2007) 22–30
Hearing Research
www.elsevier.com/locate/heares

Research paper

Tuning properties of turtle auditory nerve fibers: Evidence for suppression and adaptation

Michael G. Sneary [a,*], Edwin R. Lewis [b]

[a] Department of Biological Sciences, San Jose State University, San Jose, CA 95192-0100, USA
[b] Department of Electrical Engineering and Computer Science, University of California, Berkeley, CA 94720, USA

Received 27 July 2005; received in revised form 15 December 2006; accepted 19 December 2006
Available online 20 January 2007

Abstract

Second-order reverse correlation (second-order Wiener-kernel analysis) was carried out between spike responses in single afferent units from the basilar papilla of the red-eared turtle and band limited white noise auditory stimuli. For units with best excitatory frequencies (BEFs) below approximately 500 Hz, the analysis revealed suppression similar to that observed previously in anuran amphibians. For units with higher BEFs, the analysis revealed dc response with narrow-band tuning centered about the BEF, combined with broad-band ac response at lower frequencies. For all units, the analysis revealed the relative timing and tuning of excitation and various forms of inhibitory or suppressive effects.

Keywords: Turtle ear; Auditory nerve fibers; Wiener-kernel analysis; Suppression; High-order tuning

1. Introduction

During the past half century, the turtle inner ear has been the subject of numerous investigations. The effort has covered many aspects of inner ear structure and function and has brought the turtle to the forefront of comparative studies, along with the ranid frog. Not surprisingly, the auditory sensor, the basilar papilla, has been the focus of most of this attention. The turtle basilar papilla took center stage in auditory research when Fettiplace and Crawford and their colleagues presented an elegant series of electrophysiological studies to establish the functional parameters of turtle auditory hair cells and afferent nerve fibers (Fettiplace and Crawford, 1978; Crawford and Fettiplace, 1981a,b; Art and Fettiplace, 1984; Art et al., 1984). These studies provided a basis for understanding auditory hair cell frequency selectivity in the turtle.

Efferent axons have been observed terminating directly on turtle basilar-papillar hair cells and on afferent axons innervating those hair cells (Sneary, 1988). Art and Fettiplace (1984) and Art et al. (1984) recorded the effects of efferent-bundle shocks on hair cells and afferent nerve fiber terminals and concluded that those effects were due to the efferent terminals directly on hair cells. The shocks led to hyperpolarization in hair cells and a reduction in the sensitivities of those cells to acoustic stimuli at their characteristic frequencies. They did not produce hyperpolarization of the afferent terminals, but did nonetheless lead to cessation of spike activity. When produced in response to auditory stimuli rather than efferent-bundle stimulation, desensitization (or inhibition) such as this is always delayed (by several tens of milliseconds) relative to those stimuli.

In this paper, we present evidence for more immediate desensitization or inhibition in the turtle. Such more-immediate effects that are well known to sensory neurobiologists include fast adaptation (seen in peristimulus-time histograms as a diminution of spike rate over time following a stepwise increase in stimulus amplitude), accommodation

* Corresponding author. Tel.: +1 408 924 4854; fax: +1 408 924 4840.
E-mail address: msneary@email.sjsu.edu (M.G. Sneary).

0378-5955/$ - see front matter © 2007 Elsevier B.V. All rights reserved.
doi:10.1016/j.heares.2006.12.014

(an adjustment of threshold in response to slow changes in generator potential at spike triggers), refractoriness (a temporary threshold increase following each spike), and, for auditory scientists, one- or two-tone suppression. Suppression has been observed in auditory peripheries of mammals (Rupert et al., 1963; Frishkopf, 1964; Sachs and Kiang, 1968), birds (Temchin, 1988; Manley et al., 1985; Hill et al., 1989; Manley and Gleich, 1992), lizards (Holton, 1980), frogs (Frishkopf and Goldstein, 1963) and fish (Fay, 1986, 1990). In this paper we present the first evidence of its presence in turtles.

2. Materials and methods

The experiments upon which this paper is based were conducted in 1989 and 1990. Based on the preparation of Adrian et al. (1938) as modified by Fettiplace and Crawford (1978), red-eared turtles (*Trachemys scripta elegans*) were cold-anesthetized by immersion in ice water for approximately one-half hour and then decapitated.[1] The head was hemisected and most of the brain removed except for a small portion of the medulla including the eighth nerve where it exits the otic capsule. The isolated half-head of the animal was placed in a small chamber with a moist, oxygenated atmosphere. With the preparation maintained in this environment one could successfully record from individual nerve fibers for hours.

Recording from individual auditory nerve fibers began approximately one-half hour after completion of the preparatory dissection. Auditory stimuli were delivered via a closed field system that included a cylindrical *T* coupler filled with steel wool for attenuation of reflections. One of the two output ends of the coupler was connected through a short rubber extension tube to the skin of the animal immediately adjacent to the tympanum, so that the acoustic path within the coupler was terminated by the tympanum. The contact between the rubber tube and this extratympanal skin was sealed with silicone grease. A Bruel and Kjaer Model 4166 0.5-inch condenser microphone, tightly fitted into the other output end of the *T* coupler, was used to estimate the amplitude of the acoustic stimulus at the tympanum. The position of this microphone was symmetrical with respect to the tympanum. The input end of the *T* coupler was tightly connected to a chamber containing a Koss Pro 4XTC headphone driver. The stimulus applied to this driver was generated by a General Radio Gaussian White Noise Generator (Model 1390-B) and passed through two 1/3-octave graphic equalizers (Rane GQ-30), which were adjusted to make the output of the condenser microphone flat to within ±3 dB over the frequency range from 50–1500 Hz. This stimulus was presented continuously while spike data was accumulated. All of the experiments were carried out inside a three-walled, lab-built acoustical chamber. Over the range of frequencies used in the experiments reported here, 50–1500 Hz, the attenuation of sound passing into the chamber from the outside was greater than 50 dB.

Individual auditory nerve fibers were penetrated with 60–100 megohm microelectrodes filled with 3 M KCl. The electrode was driven into the posterior region of the eighth nerve near its point of exit from the otic capsule. The noise stimulus, as detected by the 0.5-inch microphone and the corresponding nerve fiber spikes from the microelectrode were recorded simultaneously on two channels of an audiocassette recorder (Tascam 234). This was done for a total of 37 auditory units.

At the time they were taken, the data were used to generate a reverse-correlation (REVCOR) function for each unit (Sneary and Lewis, 1989; Lewis et al., 1990). This function, equivalent to the first-order Wiener kernel, is a descriptive model of the linear behavior of the ear at sound levels in the neighborhood of the rms stimulus level. Although we have not tested its fidelity in the turtle, in frogs and mammals the REVCOR function has predicted the linear component of the ac (phase-locked) spike-rate responses to novel stimuli with extraordinary fidelity (De Boer and de Jongh, 1978; Yamada, 1997; Wolodkin et al., 1997; Lewis et al., 2002b). In this paper we revisit the same data, using it to generate the second-order Wiener kernel (Eggermont et al., 1983a,b,c; Eggermont, 1993; Van Dijk et al., 1994; Van Dijk et al., 1997a,b; Recio-Spinoso et al., 2005). That function represents the second-order nonlinear behavior of the ear. When employed as the kernel for convolution in the second-order term of the Wiener series, it predicts the second-order distortion components of the ac (phase-locked) spike-rate response and positive and negative dc spike-rate responses (shifts in the mean spike rate) (Yamada and Lewis, 1999; Lewis et al., 2002a,b). The second-order kernel also can be converted to a graph of the spectro-temporal receptive field for the unit—displaying second-order non-linear behavior in time and frequency (Lewis and van Dijk, 2004; see also Hermes et al., 1981; Eggermont et al., 1983a,b). With these tools, we hoped to extract new inferences from the old data.

3. Data analysis

The recorded data were digitized with a 10 kHz sampling rate. Spike times were identified automatically by means of a threshold and peak-detection algorithm (Yamada and Lewis, 1999). The digitized continuous noise stimuli and corresponding times of spike peaks were used to generate discrete first and second-order Wiener kernels for each auditory axon. The process of generating Wiener kernels from spike trains and a continuous noise stimulus has been described thoroughly in the literature (De Boer and Kuyper, 1968; Marmarelis and Marmarelis, 1978; De Boer and de Jongh, 1978; Van Dijk et al., 1994). The second-order kernel is computed by taking the digitized waveform

[1] All animal experiments were performed in accordance with protocols approved by the UC Berkeley Animal Care and Use Committee (Protocol number R087-1200).

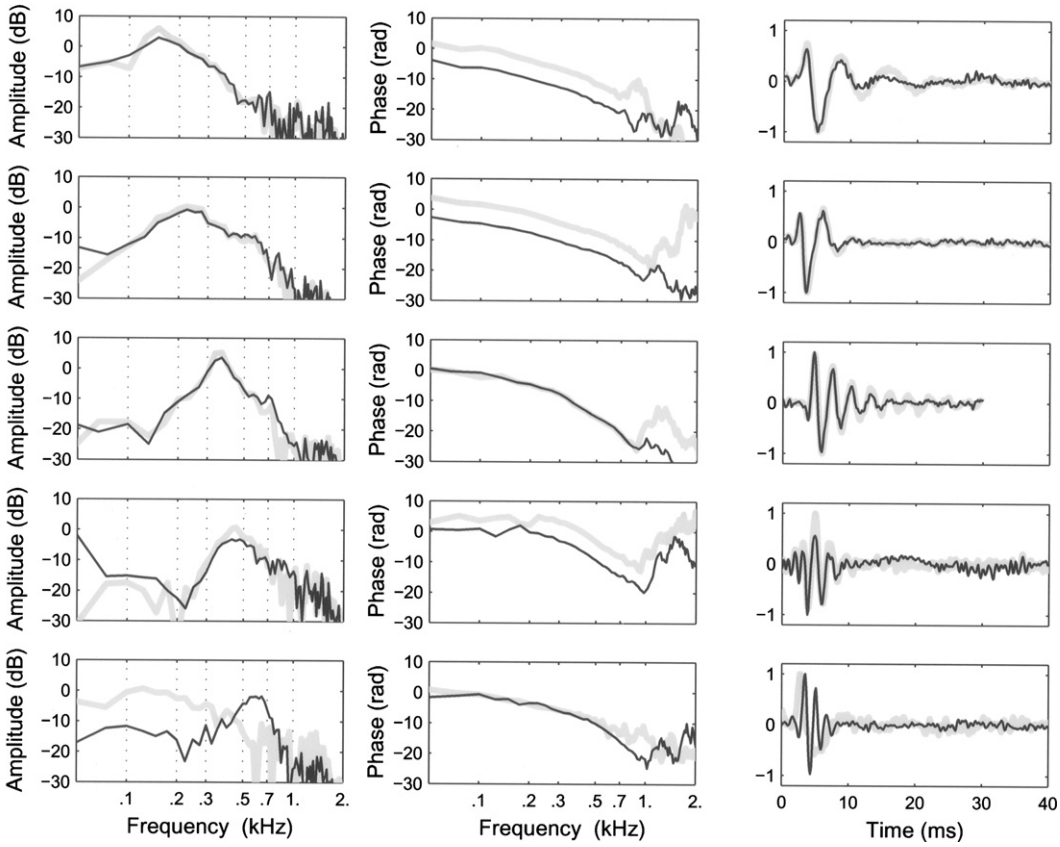

Fig. 1. First-order Wiener kernels (thick gray lines) and highest-ranking singular vectors of second-order Wiener kernels (thin black lines) for five units that span the range of best excitatory frequencies in the red-eared turtle. All of the singular vectors shown here had positive eigen values, and thus were components of the excitatory subkernels for each of the units. The temporal waveforms (normalized to have maximum absolute value of 1.0) are displayed in the right-hand column. The phase- and amplitude components of the corresponding discrete Fourier transforms are displayed in the center and left-hand columns, respectively.

(an n-element vector) that immediately preceded each spike peak, reversing it in time, forming the outer product of that waveform with itself to create an nxn matrix, taking the average of all such matrices, and subtracting from the average matrix the covariance matrix of the zero-mean noise stimulus (see Van Dijk et al., 1994). In essence, this process removes any second-order structure present in the noise stimulus at large. The resulting matrix thus provides an image of second-order structure specifically common to the noise-stimulus segments that immediately preceded spikes. For each of the 37 auditory units presented here, the number of spikes included in the analysis ranged from approximately 1500–20,000.

Through singular-value decomposition, each second-order Wiener kernel (h2) was decomposed into a set of normalized singular vectors and a set of their corresponding amplitudes (Yamada and Lewis, 1999). From these, separate excitatory and inhibitory subkernels were constructed (Lewis et al., 2002a,b). Through application of a variation of the method described in Lewis and van Dijk (2004), spectrotemporal receptive fields (power-spectral-difference functions) were also constructed directly from the whole second-order kernels (see appendix).

4. Results

Fig. 1 shows results for five units that span the range of frequency sensitivities that we observed over all 37 units. The results for these units are thoroughly representative of the results obtained for all 37 units. Each of the five units is represented by one row in the figure. For each unit, the plots in the panel on the left are the amplitude components of the discrete Fourier transforms (DFTs) of the normalized first-order Wiener kernel (h1, thick gray line) and the normalized highest ranking singular vector (SV1, thin black line) of the second-order Wiener kernel. In each of the top four rows the frequency at the peak of the DFT of h1 matched well that of SV1. We take that frequency to be the best excitatory frequency (BEF) of the corresponding unit. In the bottom row, the DFT of h1 is not well-tuned, but that of SV1 is. In that case, we take the frequency at the peak of the latter to be the unit's BEF. The middle panel shows the corresponding phase components. The panel on the right shows the normalized first-order Wiener kernel itself and the normalized highest-ranking singular vector of the second-order kernel. Note that, with the exception of the unit with the highest BEF, the two functions in each of the right-hand panels are very similar—as are the

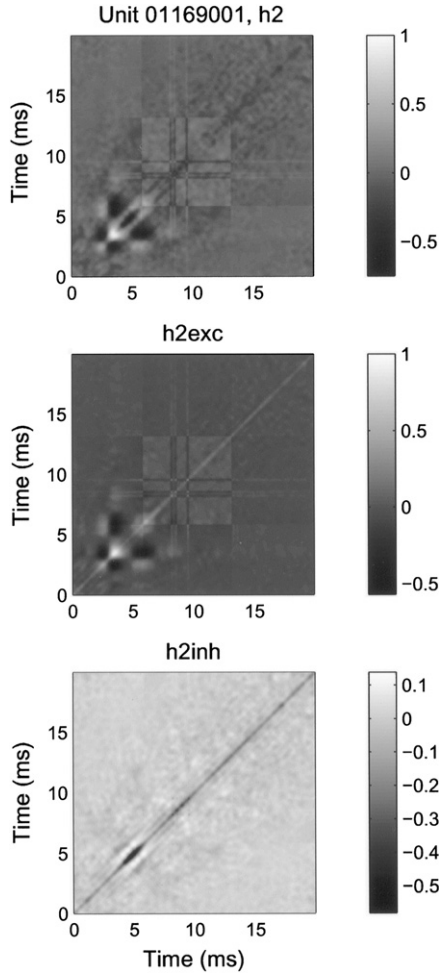

Fig. 2. Second-order Wiener kernel and its excitatory and inhibitory subkernels for turtle unit 01169001. The first-order kernel and the highest-ranking singular vector of the second-order kernel for this unit are displayed in the second row of panels in Fig. 1.

amplitude components of their DFTs. Note also that the phase components of the various DFTs span two or three cycles (2π radians per cycle).

Fig. 2 shows the second-order Wiener kernel for the unit represented in the second row of Fig. 1, along with its excitatory and inhibitory subkernels (h2exc and h2inh, respectively).[2] Observe, in the excitatory subkernel, the conspicuous pattern in the vicinity of 5 ms and its checkerboard-like appearance. In the inhibitory subkernel, note that the conspicuous pattern in this case, also in the vicinity of 5 ms, comprises parallel diagonal lines rather than a checkerboard. In singular-value decomposition this inhibitory pattern was represented by several singular vectors, no two of which formed an obvious quadrature pair and none of which was well tuned. This lack of distinct tuning among inhibitory singular vectors was observed repeatedly in the turtle units with BEFs below 500 Hz. Fig. 3 shows the power-spectral-difference function computed for the whole kernel (h2). In this figure, the boundary between pale blue and pale green (labeled zero on the vertical scale) represents the power-spectral density of the noise stimulus at large. Blue areas represent times and frequencies where the power spectral density prior to a spike was unusually low: red areas represent times and frequencies where it was unusually high.

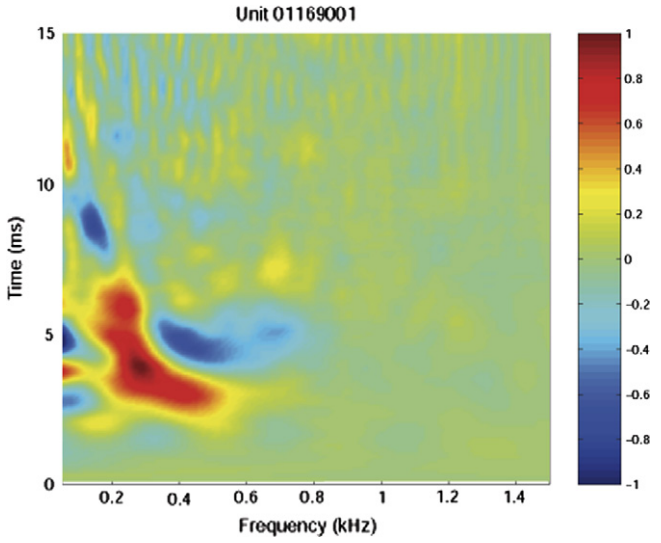

Fig. 3. Spectro-temporal receptive field (power-spectral difference function) computed from the second-order Wiener kernel in the top panel of Fig. 2. The power spectrum of the stimulus noise at large (zero on the color scale) is represented by the boundary between pale blue and pale green. The yellow to red to brown regions reflect times and frequencies where, on average, the stimulus prior to each spike had power-spectral density greater than that of the stimulus at large. The blue regions reflect times and frequencies where, on average, the stimulus prior to each spike had power-spectral density less than that of the stimulus at large.

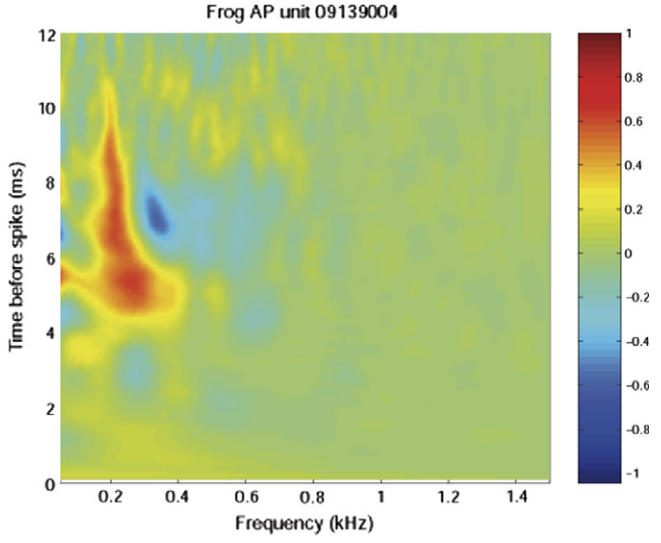

Fig. 4. Spectro-temporal receptive field computed from the second-order Wiener kernel for a unit from *Rana catesbeiana*. Interpretation of the color coding is exactly the same as that for Fig. 3.

[2] Unit labels in figures comprise a sequence of four two-digit numbers, giving month, day, year, and unit number.

Notice that there is one region in Fig. 3 where the power-spectral density of the stimulus prior to spikes was conspicuously greater than that of the noise stimulus at large (i.e., conspicuously positive power-spectral difference). From approximately 4 to 7 ms prior to each spike the spectral breadth of this region was centered approximately on 225 Hz, and corresponded well in frequency range to the peak region of the amplitude DFTs of h1 and SV1 for this unit (Fig. 1, left-hand panel of row 2). The temporal breadth of this region corresponded well with those of h1 and SV1 (Fig. 1, right-hand panel of row 2). In the neighborhood of 2.5–3 ms, the spectral breadth of this region was conspicuously greater. Overall, the region is roughly L-shaped, sloping slightly from upper left to lower right. In the inside corner of the L is a region where the power-spectral density of the stimulus prior to spikes was conspicuously less than that of the noise stimulus at large (a region of conspicuously negative power-spectral difference). To the immediate left of the L are additional regions of negative power-spectral difference, interspersed with regions of positive power-spectral difference. In fact, the L-shaped region appears to be more-or-less surrounded by regions of negative power-spectral difference. One of these occurs in the neighborhood of 8–10 ms prior to the spike, in approximately the same frequency range as the upper part of the L-shaped region. With various placements in time and frequency, the overall pattern described in this paragraph was observed repeatedly among turtle units with BEFs below 500 Hz (such as those units represented in the top four rows of Fig. 1). Going back to old data from the frog amphibian papilla (Yu, 1991; Yamada, 1997), van Dijk and Lewis found similar patterns among units with BEFs below 600 Hz (Lewis et al., 2002c). This is the frequency range over which suppression has been found in the frog amphibian papilla (Frishkopf, 1964; Frishkopf and Goldstein, 1963; Frishkopf et al., 1968). For comparative purposes we repeated the analysis of van Dyke and Lewis, modified as described in the Appendix, for several amphibian-papillar units from the American bullfrog, *Rana catesbiana*. A representative result is shown in Fig. 4.

Fig. 5 shows the second-order Wiener kernel for the unit represented by the bottom row in Fig. 1, along with its excitatory and inhibitory subkernels. Note that the dominant patterns in both subkernels comprise parallel diagonal lines, with little or no evidence of checkerboarding. For clarity, the first-order Wiener kernel (h1) and the highest-ranking singular vector (SV1) of the second-order kernel are presented separately in Fig. 6. Among the 37 units in this study, the only other that showed such a distinct difference between these two functions was 02079007, which had a BEF of approximately 700 Hz. The two units represented in Fig. 6 in fact were the only ones in this study with BEFs greater than 500 Hz. Unlike those of the other units, the main regions of positive power-spectral difference for these two units were not L-shaped, and lacked the general pattern described in the previous paragraph.

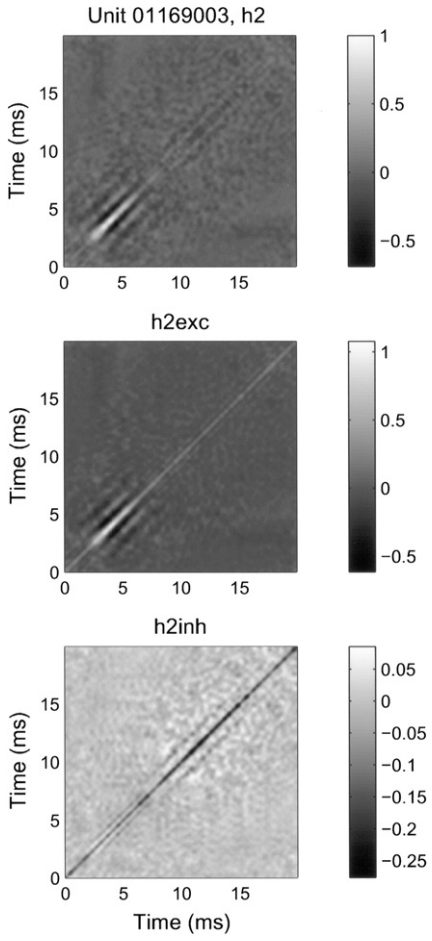

Fig. 5. Second-order Wiener kernel and its excitatory and inhibitory subkernels for turtle unit 01169003. The first-order kernel and the highest-ranking singular vector of the second-order kernel for this unit are displayed in the bottom row of panels in Fig. 1.

5. Discussion

In each of the top four units in Fig. 1, the shape of the first-order Wiener kernel (h1) is very similar to that of the highest-ranking singular vector (SV1) of the second-order kernel. We take this to imply a common underlying filter in each case (Lewis et al., 2002a,b), which we shall call the principal excitatory filter. The analysis presented in Fig. 1 tells us that when our band-limited white noise was presented to the turtle ear, each unit was most likely to respond with phase locking and/or an increase in mean (dc) spike rate when the power spectral density of the noise was high in the vicinity of a specific frequency, which we have taken to be the best excitatory frequency (BEF) (Evans, 1989; Yamada and Lewis, 1999). From top to bottom in Fig. 1, this is approximately 150 Hz, 225 Hz, 350 Hz, 450 Hz, and 650 Hz. This range of BEFs spans the behavioral audiogram of the animal (Patterson, 1966) and thus should be reasonably representative of the range of signal processing in the animal's auditory sensor, the basilar papilla.

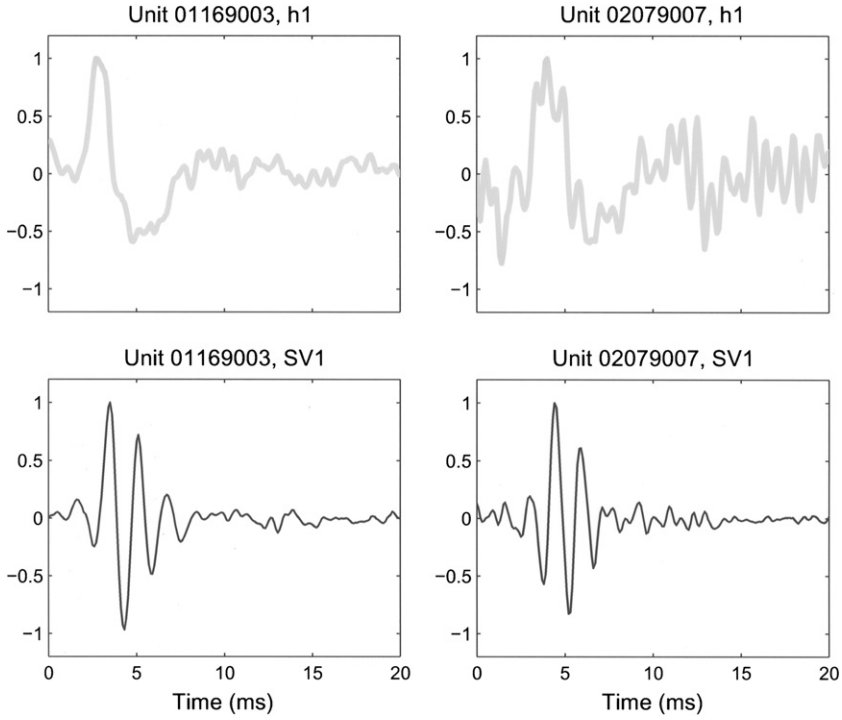

Fig. 6. First-order Wiener kernels (thick gray lines) and the highest-ranking singular vectors (thin black lines) of the second-order kernels for the two turtle units in our study with highest BEFs. Both of these singular vectors had positive eigenvalues (and thus corresponded to excitatory processes).

While one can interpret the waveforms and DFTs in Fig. 1 simply as consequences of data analysis, he or she can go one step further by taking the waveforms themselves to be time inverted-replicas of the impulse responses of the peripheral filters associated with the corresponding units. There are sound mathematical bases for this interpretation (De Boer and de Jongh, 1978; Yu, 1991; Wolodkin, 1996). Thus one would expect the linear component of any phase-locked (ac) response of a unit to be predicted by a linearly-filtered version of the corresponding stimulus waveform, the filter itself being the principal excitatory filter, as defined in the previous paragraph. The expectation has been met every time it has been tested in the vertebrate ear (De Boer and de Jongh, 1978; Carney and Yin, 1988; Wolodkin et al., 1997; Lewis et al., 2002b). The checkerboard pattern in the excitatory subkernel for the low-BEF unit in Fig. 2, then, would imply that the predominant second-order contribution from the principal excitatory filter is second-order distortion of that linearly filtered waveform (i.e., distortion of the ac response) (Lewis et al., 2002a). For a repeated stimulus waveform, such as a repeated segment of band-limited noise, the outcome of this distortion would be expansion of the amplitudes of positive excursions in the corresponding peristimulus time histogram (PSTH) and compression of the amplitudes of negative excursions (Lewis et al., 2002a). The pattern of parallel lines in the excitatory subkernel for the high-BEF unit of Fig. 5, on the other hand, would imply that the predominant second-order contribution from the principal excitatory filter is a spike-rate response (positive dc response) that follows the square of the envelope of the linearly-filtered waveform (Lewis et al., 2002a). This conclusion also has been verified experimentally (Yamada and Lewis, 1999; Lewis et al., 2002b). For (lower-frequency) units with well-tuned first-order Wiener kernels, the principal excitatory filter itself would be represented by the singular vector (usually SV1) whose shape matched that of the first-order kernel. From the shapes of the principal excitatory filter functions themselves, the shapes of the amplitude components of their DFTs, and the shapes and ranges of the phase components of their DFTs, one would conclude that the underlying dynamic processes are of high order (i.e., involve the interaction of many complementary energy storage elements) (Lewis, 1988, 1992; Lewis et al., 1990; Sneary and Lewis, 1989).

The conspicuous pattern of parallel diagonal lines in the vicinity of 5 ms in the bottom panel of Fig. 2, which we saw consistently in the inhibitory subkernels of units with BEFs below 500 Hz, implies the presence of a second principal filter—a principal inhibitory or suppressive filter (Lewis et al., 2002a). If it had been available, a well-tuned quadrature pair of singular vectors for this pattern would have given us an estimate of the filter's impulse response. The impact of the filter on any stimulus waveform then could have been estimated by convolving that waveform with the impulse response. The implied corresponding second-order contribution to the instantaneous spike rate would be a negative (dc) response that followed the square of the enve-

lope of the filtered waveform. Lacking the estimate of impulse response, we still could construct the implied response component—by second-order convolution (as in the Wiener series). It will be a negative dc component, tuned by the periodicity in the pattern of parallel lines (see Lewis et al., 2002a). In a series of simulations, Lewis et al. (2002a) showed that a quadrature pair of singular vectors can be degraded by the presence of added noise, breaking up into several, more poorly tuned vectors. Noisiness in our data thus may account for the inability of our analysis to yield simple quadrature pairs from our inhibitory patterns, in spite of the distinctiveness of the latter. Nevertheless, each of those patterns carries its implications in itself; simple singular vectors are not required.

The relationships between excitation and inhibition are clarified in the spectrotemporal patterns in Fig. 3. According to Fig. 3, on average, when there was a spike at time 0, the power spectral density at 5 ms (5 ms prior to that spike) and in the vicinity of 450–700 Hz, was very much below the background level in the white noise. Assuming that this reflects a causal relationship, one would conclude that the graph implies that a 450–700-Hz stimulus can reduce the probability of a spike, and that the latency for the inhibitory or suppressive action is about 5 ms. The fact that the inhibitory pattern in the bottom panel of Fig. 2 is coincident with a large part of the excitatory pattern in the middle panel suggests that the inhibition in this case represents what is commonly called suppression. It also is clear, from both Figs. 2 and 3, that part of the excitatory pattern is not coincident with the inhibitory pattern, but occurs in closer proximity to the time of spike occurrence (between 2 and 4 ms prior to the spike). It is in this time region that the spectrum of the excitatory pattern spreads to higher frequencies (producing the base of the L-shaped spectrotemporal pattern). It actually spans some of the spectral extent of the inhibitory pattern.

From their responses to sinusoidal stimuli, Bullfrog amphibian-papillar units with BEFs below 600 Hz consistently are found to exhibit suppression. Responses to tones at BEF consistently were reduced or eliminated by presentation of tones at slightly higher frequencies (Frishkopf et al., 1968; Feng et al., 1975). Thus it is useful to consider spectrotemporal receptive fields of such bullfrog units as derived by our modified method (see Appendix). Fig. 4 shows a representative example. As with the turtle units, with BEFs below 500 Hz, one finds an inhibitory pattern coincident with the excitatory pattern. In the unit of Fig. 4, the inhibitory pattern is centered at approximately 7 ms (prior to the spike) and 350 Hz. At 7 ms, the excitatory pattern is centered at approximately 200 Hz. We take this inhibitory pattern to reflect the same suppressive effect that had been previously observed with sinusoids.

According to Fig. 3, on average, the power spectral density in the vicinity of 200 Hz and 7.5–10 ms before the spike was very much below the background level of the noise. The peak frequency (dark-blue area) is just slightly below the peak frequency of the principal excitatory filter (BEF), and may represent adaptation, accommodation, and/or refractoriness. Any one of these phenomena could produce this sort of pattern (Lewis and van Dijk, 2004). Thus the patch of spectrotemporal negativity in the vicinity of 7.5–10 ms might be interpreted as reflecting adaptation to stimuli in the vicinity of 200 Hz. With the spectral spread of excitation beneath it, one might attach similar interpretations to the patch of negativity in the vicinity of 5 ms, 450–700 Hz in Fig. 3 and that in the vicinity of 7 ms, 400 Hz in Fig. 4. This raises the intriguing problem of differentiating between adaptation and suppression in lower vertebrates (e.g., see Lewis, 1986).

As mentioned in Section 4, the general spectrotemporal pattern of Fig. 3 was representative of all turtle units with BEFs below 500 Hz. All such units exhibited an L-shaped region of excitation, a region of putative suppression and a region of putative adaptation. As implied in the various panels of Fig. 1, from one unit to another, these regions were shifted in frequency and to some extent in time. The two, higher BEF units described below lacked the L-shaped excitatory pattern and the region of putative suppression.

The pattern between 10 and 15 ms in the inhibitory subkernel of unit 01169003 (Fig. 5) seems to mirror the pattern between 3 and 8 ms in the excitatory subkernel. This suggests that while spectral components in the vicinity of 650 Hz would be excitatory if they occurred between 3 and 8 ms ago, they would be inhibitory if they occurred between 10 and 15 ms ago. This conforms to the standard expectation for adaptation, accommodation or refractoriness.

The two units of Fig. 6 differed from all of the other units in this study in the profound difference between the tuning of h1 and SV1 in each of them. The biphasic, impulse-like shape of h1 in each case implies phase locking over a broad range of lower frequencies (e.g., see the bottom left-hand panel of Fig. 1). The SV1 waveform of each of these two units, on the other hand, reflects relatively narrow tuning for dc response at a relatively high BEF. These waveforms are not unlike the impulse responses of electronic filters designed to be selective in frequency and to respond quickly in time. They are especially reflective of high order in the underlying dynamics.

Acknowledgements

Support for this research was derived from an NIH postdoctoral Individual National Research Service Award (NS07937-02) to M.S. and funding from NIH R01-00112 (NIDCD) to E.R.L. We would also like to thank Walter Yamada, Xioalong Yu and Pim van Dijk for their contributions.

Appendix

The main diagonal of an $n \times n$ second-order Wiener kernel comprises the set of elements $\{h_2(\tau,\tau)\}$ where τ ranges from 1 to n. The overall matrix can be considered to be composed of two sets of counterdiagonals (antidiagonals):

(1) an ordered set of n counterdiagonals, each of which includes one element of the main diagonal, and (2) an ordered set of $n-1$ counterdiagonals that do not include elements of the main diagonal. The Tth member of the first set of counterdiagonals is itself an ordered set $\{h_2(T+\delta/2, T-\delta/2)\}$, where δ ranges over all of the even integers in ascending order from $-2(T-1)$ to $2(T-1)$, including zero. The Tth member of the second set of counterdiagonals is the ordered set $\{h_2(T+(\delta+1)/2,\ T-(\delta-1)/2)\}$, where δ ranges over all of the odd integers in ascending order from $-2T+1$ to $2T-1$. Combining these two ordered sets (by interleaving their elements) yields a function $d(T,\delta)$, which comprises the following ordered set of elements: $\{h_2(1,2T), h_2(1,2T-1), h_2(2,2T-1), h_2(2,2T-2), \ldots,\ h_2(T,T), \ldots, h_2(2T-2,2), h_2(2T-1,2), h_2(2-1,1), h_2(2T,1)\}$, which (for a fixed value of T) is equal to a scaled version of the difference between a short-term autocorrelation of the noise stimulus, centered $T-1$ sampling intervals prior to the occurrence of a spike peak, and a short-term autocorrelation of the noise stimulus at large (Lewis and van Dijk, 2004). Fixing T and taking the discrete Fourier transform (with respect to δ) of this function yields $K\Delta S(T,\omega)$, a scaled estimate of the difference between the short-term power spectrum of the stimulus noise centered $T-1$ sampling intervals prior to the occurrence of a spike peak and the short-term power spectrum of the noise at large (Lewis and van Dijk, 2004). Because this scaled estimate is noisy, for this paper we smoothed by averaging over eleven neighboring estimates, from $T-5$ to $T+5$ and using the result for T. For all units, our sampling interval was 0.1 ms (sampling rate = 10 kHz), making the time window for our averaging equal to 1.1 ms. The averaging in Lewis and van Dijk (2004) was carried out prior to discrete Fourier transformation, which was appropriate for excitatory and inhibitory patterns comprising lines parallel to the main diagonal, but not for checkerboard patterns. For the latter, averaging is appropriately carried out in the frequency domain (after discrete Fourier transformation), as we did here. By virtue of the manner in which h_2 is constructed, $d(T,\delta)$ always is symmetric with respect to δ (about $\delta=0$). Prior to Fourier transformation, for each value of T, $d(T,\delta)$ was zero padded to make a 1024-element vector, and then expressed as an even, circular function of δ. Consequently, its discrete Fourier transform contained only (positive or negative) real values. In Figs. 3 and 4 the averages of these values, taken over the 1.1 ms windows in T, were plotted against T and frequency ($\omega/2\pi$).

References

Adrian, E.D., Craik, K.J.W., Sturdy, R.S., 1938. The electrical response of the auditory mechanism in cold-blooded vertebrates. Proc. R Soc. B 125, 435–455.

Art, J.J., Fettiplace, R., 1984. Efferent desensitization of auditory nerve fibre responses in the cochlea of the turtle *Pseudemys scripta elegans*. J. Physiol. 356, 507–523.

Art, J.J., Fettiplace, R., Fuchs, P.A., 1984. Synaptic hyperpolarization and inhibition of turtle cochlear hair cells. J. Physiol. 356, 525–550.

Carney, L.H., Yin, C.T., 1988. Temporal coding of responses by low-frequency auditory nerve fibers: single-fiber responses and a population model. J. Neurophysiol. 60, 1653–1677.

Crawford, A.C., Fettiplace, R., 1981a. An electrical tuning mechanism in turtle cochlear hair cells. J. Physiol. 312, 377–412.

Crawford, A.C., Fettiplace, R., 1981b. Non-linearities in the responses of turtle hair cells. J. Physiol. 315, 317–338.

De Boer, E., de Jongh, H.R., 1978. On cochlear encoding: potentialities and limitations of the reverse correlation technique. J. Acoust. Soc. Am. 63, 115–135.

De Boer, E., Kuyper, P., 1968. Triggered correlation. IEEE Trans. BME 15, 169–179.

Eggermont, J.J., 1993. Wiener and Volterra analyses applied to the auditory system. Hear. Res. 66, 177–201.

Eggermont, J.J., Aertsen, A.M.H.J., Johannesma, P.I.M., 1983a. Quantitative characterization procedure for auditory neurons based on the spectro-temporal receptive field. Hear. Res. 10, 167–190.

Eggermont, J.J., Aertsen, A.M.H.J., Johannesma, P.I.M., 1983b. Prediction of the responses of auditory neurons in the midbrain of the grass frog based on the spectro-temporal receptive field. Hear. Res. 10, 191–202.

Eggermont, J.J., Johannesma, P.I.M., Aertsen, A.M.H.J., 1983c. Reverse correlation methods in auditory research. Q. Rev. Biophys. 16, 167–190.

Evans, E.F., 1989. Cochlear filtering: a view seen through the temporal discharge patterns of single cochlear nerve fibers. In: Wilson, J.P., Kemp, D.T. (Eds.), Cochlear Mechanisms, Structure, Function and Models. Plenum, New York, pp. 241–250.

Fay, R.R., 1986. Frequency selectivity, adaptation and suppression in goldfish auditory nerve fibers. In: Moore, B.C., Patterson, R.D. (Eds.), Auditory Frequency Selectivity. Plenum Press, New York, pp. 137–145.

Fay, R.R., 1990. Suppression and excitation in auditory nerve fibers of the goldfish, *Crassius auratus*. Hear. Res. 48, 93–110.

Feng, A.S., Narins, P.M., Capranica, R.R., 1975. Three populations of primary auditory fibers in the bullfrog (*Rana catesbeiana*): their peripheral origin and frequency sensitivity. J. Comp. Physiol 100, 221–229.

Fettiplace, R., Crawford, A.C., 1978. The coding of sound pressure and frequency in cochlear hair cells of the terrapin. Proc. Roy. Soc. Lond. B. 203, 209–218.

Frishkopf, L.S., 1964. Excitation and inhibition of primary auditory neurons in the little brown bat. J. Acoust. Soc. Am. 36, 1016.

Frishkopf, L.S., Goldstein Jr., M.H., 1963. Response to acoustic stimuli from single units in the eighth nerve of the bullfrog. J. Acoust. Soc. Am. 35, 1219–1228.

Frishkopf, L.S., Capranica, R.R., Goldstein, M.H., 1968. Neural coding in the frog's auditory system—a teleological approach. Proc. I.E.E.E. 56, 969–980.

Hermes, D.J., Aertsen, A.M.H.J., Johannesma, P.I.M., Eggermont, J.J., 1981. Spectro-temporal characteristics of single units in the auditory midbrain of the lightly anesthetized grass frog (*Rana temporaria*) investigated with noise stimuli. Hear. Res. 5, 147–178.

Hill, K.G., Mo, J., Stange, G., 1989. Excitation and suppression of primary auditory fibers in the pigeon. Hear. Res. 39, 37–48.

Holton, T., 1980. Relations between frequency selectivity and two-tone rate suppression in lizard cochlear nerve fibres. Hear. Res. 2, 21–38.

Lewis, E.R., 1986. Adaptation, suppression and tuning in amphibian acoustical fibers. In: Moore, B.J.C., Patterson, R.D. (Eds.), Auditory Frequency Selectivity. Plenum, New York, pp. 129–136.

Lewis, E.R., 1988. Tuning in the bullfrog ear. Biophys. J. 53, 441–447.

Lewis, E.R., 1992. Convergence of design in vertebrate acoustic sensors. In: Webster, D.B., Fay, R.R., Popper, A.N. (Eds.), The Evolutionary Biology of Hearing. Springer Verlag, New York, pp. 163–184.

Lewis, E.R., van Dijk, P., 2004. New variations on the derivation of spectro-temporal receptive fields for primary auditory afferent axons. Hear. Res. 189, 120–136.

Lewis, E.R., Sneary, M.G., Yu, X., 1990. Further evidence for tuning mechanisms of high dynamic order in lower vertebrates. In: Dallos, P., Geisler, C.D., Matthews, J.W., Ruggero, M.A., Steele, C.R. (Eds.), The

Mechanics and Biophysics of Hearing, Lecture Notes in Biomathematics, Vol. 87. Springer-Verlag, New York, pp. 139–146.

Lewis, E.R., Henry, K.R., Yamada, W.M., 2002a. Tuning and timing of excitation and inhibition in primary auditory nerve fibers. Hear. Res. 171, 13–31.

Lewis, E.R., Henry, K.R., Yamada, W.M., 2002b. Tuning and timing in the gerbil ear: Wiener kernel analysis. Hear. Res. 174, 206–221.

Lewis, E.R., van Dijk, P., Yamada, W.M., 2002c. Suppression of frog amphibian-papillar axons. J. Acoust. Soc. Am. 112, 2229.

Manley, G.A., Gleich, O., 1992. Evolution and specialization of function in the avian auditory periphery. In: Webster, D.B., Fay, R.R., Popper, A.N. (Eds.), The Evolutionary Biology of Hearing. Springer-Verlag, New York, pp. 561–583.

Manley, G.A., Gleich, O., Leppelsack, H.J., Oekinghaus, H., 1985. Activity patterns of cochlear ganglion neurones in the starling. J. Comp. Physiol. A. 157, 161–181.

Marmarelis, P.Z., Marmarelis, V.Z., 1978. Analysis of Physiological Systems: The White Noise Approach. Plenum, New York.

Patterson, W.C., 1966. Hearing in the turtle. J. Aud. Res. 6, 453–464.

Recio-Spinoso, A., Temchin, A.N., van Dijk, P., Fan, Y-H., Ruggero, M.A., 2005. Wiener-kernel analysis of responses to noise of chinchilla auditory-nerve fibers. J. Neurophysiol. 93, 3615–3634.

Rupert, A., Moushegian, G., Galambos, R., 1963. Unit responses from auditory nerve of the cat. J. Neurophysiol. 26, 449–465.

Sachs, M.B., Kiang, N.Y.-S., 1968. Two-tone inhibition in auditory nerve fibers. J. Acoust. Soc. Am. 43, 1120–1128.

Sneary, M.G., 1988. Auditory receptor of the red-eared turtle: II. Afferent and efferent synapses and innervation patterns. J. Comp. Neurol. 276, 588–606.

Sneary, M.G., Lewis, E.R., 1989. Response properties of turtle auditory afferent nerve fibers: evidence for high-order tuning mechanism. In: Wilson, J.P., Kemp, D.T. (Eds.), Cochlear Mechanisms, Structure, Function and Models. Plenum, New York, pp. 235–240.

Temchin, A.N., 1988. Unusual discharge patterns of single fibers in the pigeon's auditory nerve. J. Comp. Physiol. A 163, 99–115.

Van Dijk, P., Wit, H.P., Segenhout, J.M., Tubis, A., 1994. Wiener kernel analysis of inner ear function in the American bullfrog. J. Acoust. Soc. Am. 95, 904–919.

Van Dijk, P., Wit, H.P., Segenhout, J.M., 1997a. Dissecting the frog inner ear with Gaussian noise. I. Application of high-order Wiener kernel analysis. Hear. Res. 114, 229–242.

Van Dijk, P., Wit, H.P., Segenhout, J.M., 1997b. Dissecting the frog inner ear with Gaussian noise. II. Temperature-dependence of inner-ear function. Hear. Res. 114, 243–251.

Wolodkin, G.J. 1996. System identification for a class of structured nonlinear systems. Ph.D. Dissertation, Department of Electrical Engineering and Computer Science, University of California, Berkeley.

Wolodkin, G., Yamada, W.M., Lewis, E.R., Henry, K.R., 1997. Spike rate models for auditory fibers. In: Lewis, E.R., Long, G.R., Lyon, R.F., Narins, P.F., Steele, C.R., Hecht-Poinar, E. (Eds.), Diversity in Auditory Mechanics. World Scientifc Press, Singapore, pp. 104–110.

Yamada, W.M., 1997. Second-order Wiener Kernel Analysis of auditory afferent axons of the North American Bullfrog and Mongolian Gerbil responding to noise. Ph.D. Dissertation. Graduate Group in Neurobiology. University of California, Berkeley, CA.

Yamada, W.M., Lewis, E.R., 1999. Predicting the temporal response of non-phase-locking bullfrog auditory units to complex acoustic waveforms. Hear. Res. 130, 155–170.

Yu, X.L., 1991. Signal processing mechanics in bullfrog ear inferred from neural spike trains. Ph.D. Dissertation, Department of Electrical Engineering and Computer Science, University of California, Berkeley.